Extracting Transient Phase-Amplitude Coupling from Resting-State EEG Signals

A. Er, M. Le Van Quyen, J. Dauguet, V. Marchand-Pauvert* and G. Marrelec*
Sorbonne Université, CNRS, INSERM, Laboratoire d'Imagerie Biomédicale, LIB, F-75006, Paris, France

***Abstract*—Electroencephalography (EEG) allows us to observe brain activity through electrical signals. Phase-amplitude coupling (PAC) is a way to analyze EEG data by focusing on the interaction between the low- and high-frequency components of these signals. However, PAC analyses are often challenged by various methodological issues. We here propose a novel approach which alleviates these issues. Our method has the following features: (i) it addresses the transient nature of coupling through data epoching; (ii) it ensures the presence of low-frequency oscillations through peak detection in the power spectrum; (iii) it applies adaptive high-frequency filtering; and (iv) it performs statistical validation using surrogate data. The efficiency of our method is demonstrated through both a simulation study and the analysis of experimental EEG data, offering new insights into the intricate workings of brain signal interactions.**

***Index Terms*—brain oscillations; electroencephalography (EEG); resting-state EEG; phase-amplitude coupling; cross-frequency coupling**

I. Introduction

Electroencephalography (EEG) is a non-invasive brain exploration technique that makes it possible to record electrical signals resulting from neuronal activity. These recordings are driven by oscillations arising from the synchronized activity of neuronal populations. Observed oscillations can vary in their frequency, with distinct bands like delta (1–4 Hz), theta (4–8 Hz), alpha (8–12 Hz), beta (12–30 Hz), and gamma (above 30 Hz), each associated with specific functions [1]. In particular, it is hypothesized that high-frequencies could be associated with localized brain activity, while lower frequencies may be a signature of large-scale interactions between distant brain areas [1]. Since one could expect a coordination between local activities and large-scale interactions, it has been suggested that low- and high-frequency bands could interact with each another, a phenomenon called cross-frequency coupling (CFC) [2]. A particular form of CFC, called phase amplitude coupling (PAC), analyzes the relationship between the phase of a low-frequency signal, typically in the theta and alpha bands, and the amplitude of a high-frequency signal, commonly in the beta and gamma ranges. PAC can be quantified using various methods [3]–[6]. It has been related to processes like attention [7], decision making [8], synaptic plasticity [9], and has been investigated as a biomarker in clinical alterations [10]–[12].

This project has been funded by the French National Research Agency (ANR-21-CE37-0033-02 FREQUALS). Please address correspondance to Alper Er (alper.er@sorbonne-universite.fr).

* both authors contributed equally to the manuscript.

Various methodological issues still hamper PAC analyses [13]–[16]. First, the transient nature of coupling means that this phenomenon should be studied over relatively short time scales (issue I). Second, PAC only has a meaning in the case of low-frequency oscillatory signals, i.e., in association with a clear peak in the corresponding range of the power spectral density (PSD) (issue II). Third, an overly broad or narrow bandwidth for the high-frequency filtering can respectively introduce unrelated neural activities or overlook amplitude modulations (issue III). Fourth, raw values of PAC are often hard to interpret and their relevance in terms of coupling can usually only be determined though a statistical analysis (issue IV).

In the present abstract, we are interested in the extraction of PAC from resting-state EEG signals, focusing on potential interactions between the theta-alpha band (4–12 Hz, for the low-frequency oscillations) and the gamma band (30–60 Hz, for the high-frequency oscillations). To our knowledge, no method proposed so far [17]–[19] simultaneously solves the four issues mentioned above. We propose a detailed pipeline that attempts to address these concerns.

The outline of the abstract is the following. We first introduce the details of our approach (Section II). We then validate it through data simulations (Section III) and finally illustrate it on experimental EEG data (Section IV).

II. Methods

Our PAC method is structured into 4 successive steps. We begin by decomposing our signal into epochs of short duration (Section II-A), addressing issue I. For each epoch, we calculate the PSD and extract the low-frequency peaks; we only keep epochs that show one or several clear peaks in the low-frequency band of interest and focus on low-frequency intervals within the extracted peaks (Section II-B), thereby addressing issue II. We then perform PAC analysis using an adaptive high-frequency window (Section II-C), addressing issue III. Finally, we identify significant PAC by performing surrogate analysis, correcting for multiple comparisons with the pixel-based maximum statistic (Section II-D), addressing issue IV.

A. Data Epoching

The initial step of our pipeline involves the segmentation of the resting-state EEG signal into epochs of 3-second duration. The choice of 3 s epochs offers a good compromise between

sensitivity to changes and reliability of PSD estimation. Indeed, by using short time frames, we enhance our ability to detect subtle, yet significant, transient PAC. This segmentation also limits the influence of non-stationarities in the EEG recordings. A 3 s duration (corresponding to at least 12 cycles for the considered low-frequency band) is also long enough to allow proper estimation of the PSD in the subsequent step. At the end of this stage, the signal is segmented into E epochs.

B. Low-Frequency Peak Detection

We consider the presence of one or several peaks in the low-frequency range of the PSD to be a prerequisite for PAC analysis [13]. Following the data epoching step, we calculate the PSD between 2 and 70 Hz for each epoch $e \in \{1, \ldots, E\}$, by using the Welch method [20] and extract the peaks (as intervals of the form $[\nu - \Delta\nu, \nu + \Delta\nu]$, where ν is a local maximum and $2\Delta\nu$ a width) standing out of an expected $1/f$ noise background [21]. We then keep the K_e peaks $\nu_{ek} \pm \Delta\nu_{ek}$, $k = 1, \ldots, K_e$, with a nonempty overlap with the low-frequency range of interest (4–12 Hz). Epochs without at least one peak in the range (corresponding to $K_e = 0$) are discarded.

C. Assessing Phase Amplitude Coupling

The following procedure is applied to each epoch e with at least one peak in the low-frequency range ($K_e \geq 1$). We split both the low- and high-frequency ranges into 30 frequency steps each:

$$(f_1^{\mathrm{LF}} = 4, \ldots, f_{30}^{\mathrm{LF}} = 12) \text{ and } (f_1^{\mathrm{HF}} = 30, \ldots, f_{30}^{\mathrm{HF}} = 60). \tag{1}$$

We consider only the f_i^{LF}'s that belong to an identified peak, i.e., for which there exists $k \in \{1, \ldots, K_e\}$ such that

$$\nu_{ek} - \Delta\nu_{ek} \leq f_i^{\mathrm{LF}} \leq \nu_{ek} + \Delta\nu_{ek}. \tag{2}$$

To extract the low-frequency component around f_i^{LF}, the original signal is filtered by application of a bandpass filter around f_i^{LF} with a bandwidth of 2 Hz. For the high-frequency signal, we apply a bandpass filter as well around f_j^{HF} with an adaptive bandwidth of $2f_i^{\mathrm{LF}}$ [17]. For each pair $(f_i^{\mathrm{LF}}, f_j^{\mathrm{HF}})$, a Hilbert transform is applied to the low-frequency signal to extract the time course of phases and to the high-frequency signal to extract the time course of amplitudes. Next, we quantify the PAC between phase and amplitude as $\mathrm{MI}_e(f_i^{\mathrm{LF}}, f_j^{\mathrm{HF}})$ using the Kullback–Leibler (KL) divergence-based Modulation Index (MI) method [5]. MI bins phases and, for each bin, computes the average of amplitudes whose corresponding phases belong to that bin. The averages are then normalized so that their sum is equal to 1. Departure of the normalized averages from equality is then quantified as the KL-divergence between these values and identical normalized averages. Repetition of this operation for each pair $(f_i^{\mathrm{LF}}, f_j^{\mathrm{HF}})$ yields a matrix called comodulogram. From this comodulogram, we finally calculate $\max_{ij} \mathrm{MI}_e(f_i^{\mathrm{LF}}, f_j^{\mathrm{HF}})$, the maximum value of PAC over all frequencies considered.

D. Surrogate Data Analysis

In the final step, we evaluate the statistical significance of calculated PAC for each epoch as follows [22, Chap. 33.6]. We compute an approximate null distribution using 200 surrogate datasets, each created by circularly shifting the amplitude envelope at a random point, thereby disrupting any intrinsic coupling between low-frequency phase and high-frequency amplitude. For each surrogate dataset, PAC is calculated over the same range of low- and high- frequencies as the original data, and then the maximum value is extracted. Pooling all surrogate maximum values, we obtain a (surrogate) histogram approximating the distribution of the maximum value of PAC under the null hypothesis of no coupling. We then compare the actual PAC value obtained for the given epoch to its corresponding distribution, yielding a p-value against the assumption that there is no coupling in a given epoch. An epoch is deemed to have significant PAC if its p-value is below the $\alpha = 0.05$ threshold.

E. Implementation

Implementation of the method was carried out using Python 3.9. The core data structures used for the signals, data epoching and PSD analysis were provided by MNE-Python [23]. For the low-frequency peak detection, we incorporated the FOOOF algorithm [21]. Additionally, we used filtering functions provided by Pactools—a Python package specializing in PAC [17]. Regarding surrogate data analysis, we used multi-thread processing in order to optimize the calculation time.

III. Simulation study

The procedure introduced in Section II was evaluated using synthetic data. We here present the data generation scheme (Section III-A), detail our analysis (Section III-B), explain our assessment method (Section III-C) and state the main results (Section III-D).

A. Data

Our objective was to generate signals with specific features that we hoped would satisfactorily mimic those of real data. In particular, while PAC is a phenomenon that is most likely not stationary over time, we assumed that it could be approximated by a succession of stationary processes over windows of varying duration. During each window, the simulated signal may or may not exhibit power in the low- and high-frequency bands. Moreover, in case of power in both bands, there may or may not be PAC.

Table I summarizes the values for the parameters used in simulation. We defined M levels of modulation intensity $\lambda_m^{(0)}$, $m = 1, \ldots, M$. For each level m, we simulated R resting-state signals of duration 5 min each sampled at a rate of f_s Hz. Each 5 min simulated signal $s_{mr}(t)$, $1 \leq r \leq R$, was decomposed into short windows of random duration sampled uniformly in $[\tau_{\min}, \tau_{\max}]$. Within each window w, the signal $s_{mrw}(t)$ could contain a low-frequency component s_{mrw}^{LF} (with probability π^{LF}), as well as a high-frequency component s_{mrw}^{HF}

TABLE I
SIMULATION STUDY. VALUES OF PARAMETERS USED FOR THE SIMULATION.

Parameter	M	$\lambda_1^{(0)}$	$\lambda_2^{(0)}$	$\lambda_3^{(0)}$	$\lambda_4^{(0)}$	R	f_s	$\tau_{\min}$	$\tau_{\max}$	π^{LF}	π_θ	π_α	$\Delta\nu^{\mathrm{LF}}$	π^{HF}	π_c	σ^2
Value	4	0.5	1	2	3	100	256 Hz	2.5 s	6 s	2/3	1/2	1/2	1 Hz	1/2	2/3	0.5

(with probability π^{HF}). The presence of the low- and high-frequency components was decided independently from each other.

If present, the low-frequency component $s^{\mathrm{LF}}_{mrw}(t)$ could be either in the theta band (with probability π_θ) or in the alpha band (with probability $\pi_\alpha = 1 - \pi_\theta$). The center frequency ν^{LF}_{mrw} of the low frequency was then sampled with a uniform distribution, either in $[4, 8]$ Hz for the theta band or in $[8, 12]$ Hz for the alpha band. The exact signal was then obtained as a filtered version of Gaussian white noise, the filter being a finite impulse response filter with center frequency ν^{LF}_{mrw} and width $\Delta\nu^{\mathrm{LF}}$. This allowed to generate a low-frequency component s^{LF}_{mrw} with controlled frequency and varying amplitude [17].

If present, the high-frequency signal s^{HF}_{mrw} was modeled as a sine with frequency ν^{HF}_{mrw} set uniformly in $[30, 60]$ Hz.

If the window w contained both a low-frequency and a high-frequency component, we added a coupling $c_{mrw}(t)$ between both components with probability π_c. If present, the coupling took the form of a sigmoid function [17]:

$$c_{mrw}(t) = \frac{1}{1 + \exp[-\lambda_{mrw} s^{\mathrm{LF}}_{mrw}(t)]}, \tag{3}$$

where $\lambda_{mrw} = \lambda_m^{(0)}$ is the modulation intensity, and the high-frequency component was obtained as

$$s^{\mathrm{HF}}_{mrw}(t) = c_{mrw}(t) \sin(2\pi\nu^{\mathrm{HF}}_{mrw} t). \tag{4}$$

By contrast, in the absence of coupling, we used the same formulas with $\lambda_{mrw} = 0$, leading to $c_{mrw}(t) = 1/2$.

Each $s_{mrw}(t)$ was then set as the sum of $s^{\mathrm{LF}}_{mrw}(t)$ and $s^{\mathrm{HF}}_{mrw}(t)$, and the total 5 min signal $s_{mr}(t)$ was obtained by concatenating all $s_{mrw}(t)$, $1 \leq w \leq W$. To this signal, we finally added a $1/f$ noise with variance σ^2 [24].

B. Analysis

For each 5 min simulated signal, the analysis had to deal with $5 \times 60/3 = 100$ 3 s epochs. For each epoch, we obtained a value for the maximum PAC Modulation Index (maxMI), $\max_{ij} \mathrm{MI}(f_i^{\mathrm{LF}}, f_j^{\mathrm{HF}})$ (set to 0 when the epoch had no power in the low-frequency range of interest), as well as the result of a significance test against the null hypothesis that there is no coupling within the given epoch (threshold of $\alpha = 0.05$).

C. Assessment

To assess the behavior of our method, we used the ground truth to compute the coupling time fraction of each epoch, that is, the fraction of time spent in coupling within that epoch. This quantity varied from 0 (indicating no coupling during the epoch) to 1 (indicating the presence of coupling throughout the epoch). Notably, a fraction of 1 may correspond to two distinct sets of parameters for the low- and high-frequency components. We then pooled maxMI across epochs with similar coupling time fractions, using the following bins: 0 (only epochs with no coupling), 0^+–0.2 (epochs with coupling time fraction strictly larger than 0 and lower than or equal to 0.2), 0.2^+–0.4, 0.4^+–0.6, 0.6^+–0.8, and 0.8^+–1. For each bin, we also computed the ratio of epochs within that bin that were detected as significant.

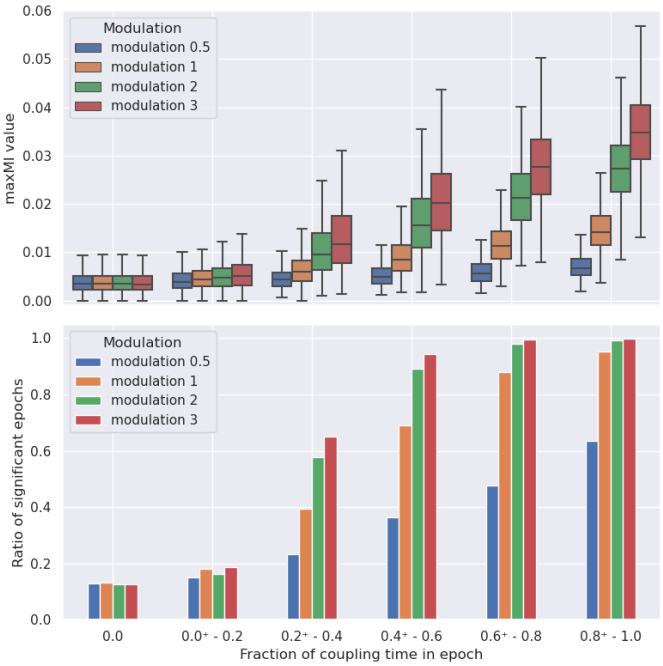

Fig. 1. **Simulation study.** Results of analysis. Boxplot of maxMI (top) and ratio of significant epochs (bottom) as a function of within-epoch coupling time fraction.

D. Results

Fig. 1 illustrates the results of our analysis. As expected, maxMI was an increasing function of both the modulation intensity and the within-epoch coupling time fraction.

The fraction of significant epochs exhibited a similar behavior. For a within-epoch coupling time of 0, we only observed false positives, about 10%. For epochs featuring coupling, the fraction of significant epochs increased with increasing modulation intensity as well as with coupling time fraction.

IV. EXPERIMENTAL STUDY

In this section, we applied our analysis pipeline to experimental EEG recordings. We detail the employed dataset in Section IV-A, expound our analytical methodology in

Section IV-B, and subsequently present our findings in Section IV-C.

A. Data

Data used is a part of a protocol which was approved by the INSERM Ethics Committee (protocol #C17-70) and national ethical authorities (CPP Ouest II Angers, n°18.07.11.57804 2018/58; RCB 2018-A00789-52). Experiment involved a 5 min resting-state EEG recording (4 kHz sampling rate, bandpass 0.03–1330 Hz) of a healthy participant (female, age 31, right-handed). The Neuromag® TRIUX system, an EEG cap with 74-Ag/AgCl electrodes following 10–20 placement, was used. The participant was instructed to keep her eyes closed and minimize movement.

We focused on signal recorded from the C3 electrode, which is positioned above the left primary motor cortex. This electrode is particularly relevant for monitoring brain activity related to sensorimotor processing of a right-handed individual at rest [25].

Preprocessing of the raw EEG data was conducted using MNE-Python [23], involving downsampling to 256 Hz, 50 Hz notch filtering, and 1–70 Hz bandpass. Faulty channels were interpolated, and signals were average-referenced. Visual inspection identified corrupt data segments, and Independent Component Analysis (ICA) [26] was applied to remove artifacts from muscle, eye, and cardiac activity.

B. Analysis

PAC analysis pipeline was applied to the preprocessed empirical EEG data. The 5 min resting state signal was segmented into 100 3 s epochs. To assess the performance of the multi-thread processing, we monitored processing time and memory usage during surrogate data analysis with a number of threads varying from 1 to 8. Computations were performed on a computer with Intel® Xeon(R) Silver 4216, 2.10 GHz CPU, and 64 GB 3200 MHz DDR4 RAM.

C. Results

Fig. 2 displays a comparison of processing time and memory usage during surrogate analysis as a function of the number of threads. We observed an exponential decay for time and a positive linear relationship for memory usage.

Fig. 3 illustrates results of PAC analysis applied to one particular epoch. The p-value corresponding to the observed maxMI was lower than the 0.05 significance threshold, indicating the presence of significant PAC.

Fig. 4 shows a summary of analysis for all epochs. PSD analysis resulted in 3% of epochs without peak in the 4–12 Hz frequency range, compared with 97% with at least one peak. Of epochs with significant low-frequency power, we found that maxMI ranged from 0.0015 to 0.012. 8% of epochs were detected with significant coupling. Importantly, we did not find a purely monotonic relationship between maxMI and p-value, as similar maxMI values across different epochs could translate into quite different p-values. In other words, raw values of maxMI were not per se good indicators of the presence or absence of coupling.

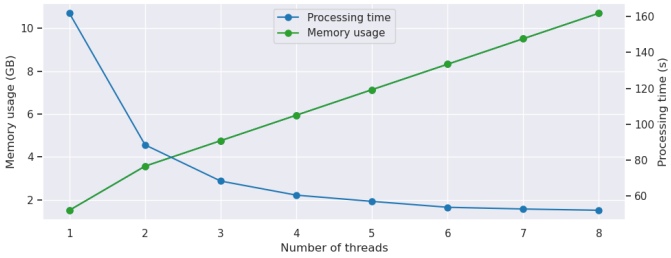

Fig. 2. **Experimental data.** Performance of multi-thread processing. Memory usage (green line, scale on the left side) and processing time (blue line, scale on the right side) as a function of the number of threads used for surrogate analysis.

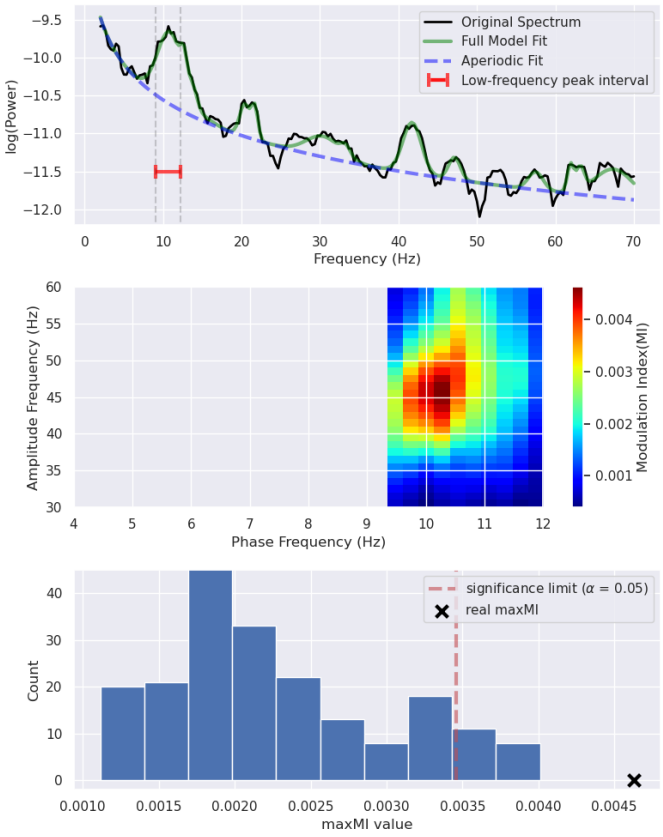

Fig. 3. **Experimental data.** Example of intermediary steps for a given epoch (red dots in Fig. 4). Top: PSD and low-frequency peak detection with FOOOF algorithm. Middle: PAC comodulogram between low-frequency phase and high-frequency amplitude, focusing on the low-frequency range corresponding to a peak in the PSD. Bottom: Actual maxMI compared with histogram of surrogate maxMI.

V. Discussion

In our study, we introduced an efficient pipeline for extracting transient PAC from resting-state EEG signals, addressing key challenges with data epoching (issue I), low-frequency peak detection (issue II), adaptive high-frequency filtering (issue III), and statistical testing using surrogate data (issue IV). This approach was validated on synthetic data and illustrated on experimental data.

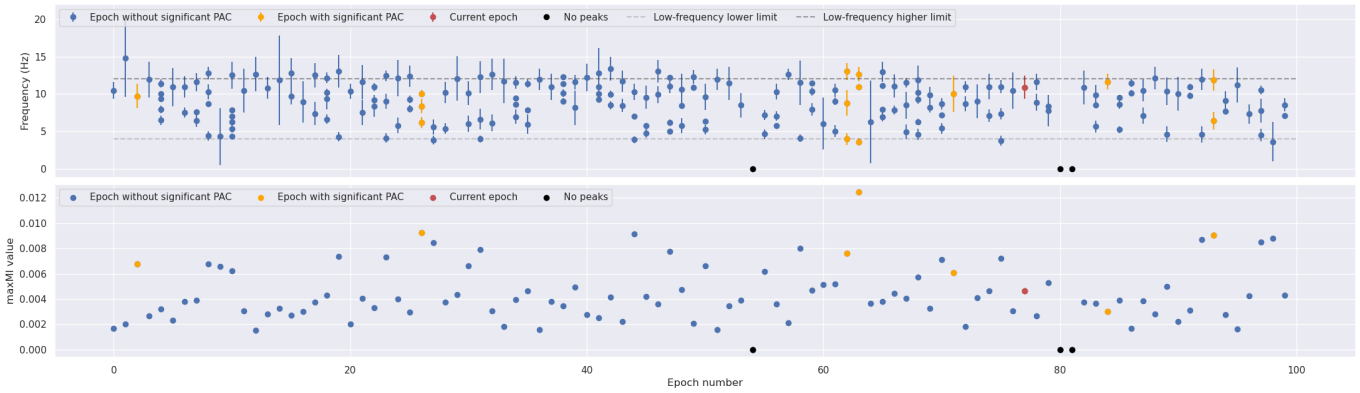

Fig. 4. **Experimental data.** Summary of analysis results for all epochs. For each epoch, detected peaks in the low-frequency band (top) and maxMI (bottom). Red dots correspond to intermediary steps illustrated in Fig. 3.

The simulation study confirmed the good behavior of our approach. In particular, it emphasized the fact that maxMI tended to increase in response to an increase in both the modulation intensity and the within-epoch coupling time fraction. This increase in maxMI was also mirrored in the growing fraction of epochs classified as significant. These results confirm the relevance of our procedure for PAC analysis.

Our procedure was also successfully applied to experimental EEG signals, illustrating the existence of the following three kinds of epochs in real data: those with no power in the low-frequency band, those with low-frequency power but no coupling, and those with both low-frequency power and coupling. While the relative ratio of these three cases is expected to vary from subject to subject, we showed that our method was able to discriminate between these three types of epochs.

In our experimental data, we observed temporal fluctuations in both the low-frequency peaks (Fig. 4, top panel) and the strength of PAC (Fig. 4, bottom panel), giving credit to the hypothesis of transient coupling (issue I). Data epoching allowed us to deal with these fluctuations separately. Additionally, low-frequency peaks were not consistently present across all epochs or did not always span the entire frequency interval of interest (issue II). Consequently, focusing on low-frequency bands where signal power was evident helped reduce the risk of misinterpretation. Furthermore, large values of raw maxMI did not consistently indicate significant coupling, confirming that the existence of PAC could not be solely determined by the raw values of maxMI (issue IV). This underscores the sensitivity of PAC analysis and emphasizes the need for caution when interpreting raw maxMI values, as well as the importance of employing appropriate statistical tests. Lastly, to address issue III, we applied variable high-frequency filtering. A more comprehensive analysis is required to fully validate this last point.

We have to keep in mind that our method summarizes a whole comodulogram with one single value. There are two common ways to perform this type of summary, by taking either the maximum of the comodulogram (i.e., maxMI), or its mean (leading to a quantity that could be called "meanMI"). In our methodology, the low-frequency range was identified using a peak detection procedure, while the high-frequency range was manually selected by the operator. Consequently, PAC was computed across potentially broad low- and high-frequency ranges. However, it is important to note that cross-frequency coupling may occur within very narrow frequency bands. Therefore, our comodulograms might display extensive areas of low PAC together with localized areas of high PAC. To effectively capture these potentially small areas of significant coupling, we chose to use maxMI rather than meanMI. We were concerned that averaging the values with meanMI could obscure these critical localized coupling events.

Regardless of the summary chosen, it is important to recognize that this approach provides only a limited view of the qualitative properties of coupling. In particular, it will not detect changes in the features of a coupling (such as frequency or modulation) nor differentiate multiple simultaneous couplings within the same epoch.

While our study primarily utilized the MI method [5] to quantify PAC, the pipeline's versatility easily allows adaptation to other methodologies [3], [4], [6] and EEG contexts as sleep EEG studies and stimulation protocols, reinforcing its wide applicability in neurophysiological research.

Finally, we hope to apply our method to a broader range of real data in the future, aiming for a more comprehensive understanding and generalizability of our findings.

ACKNOWLEDGMENT

The authors would like to thank the Center for Neuro-Imaging Research (CENIR) of the Brain and Spine Institute (ICM, Paris, France) for the acquisition of the experimental data.

REFERENCES

[1] G. Buzsáki and A. Draguhn, "Neuronal Oscillations in Cortical Networks," *Science*, vol. 304, no. 5679, pp. 1926–1929, Jun. 2004.

[2] R. T. Canolty and R. T. Knight, "The functional role of cross-frequency coupling," *Trends in Cognitive Sciences*, vol. 14, no. 11, pp. 506–515, Nov. 2010.

[3] F. Mormann, J. Fell, N. Axmacher, B. Weber, K. Lehnertz, C. E. Elger, and G. Fernández, "Phase/amplitude reset and theta–gamma interaction in the human medial temporal lobe during a continuous word recognition memory task," *Hippocampus*, vol. 15, no. 7, pp. 890–900, 2005.

[4] R. T. Canolty, E. Edwards, S. S. Dalal, M. Soltani, S. S. Nagarajan, H. E. Kirsch, M. S. Berger, N. M. Barbaro, and R. T. Knight, "High Gamma Power Is Phase-Locked to Theta Oscillations in Human Neocortex," *Science*, vol. 313, no. 5793, pp. 1626–1628, Sep. 2006.

[5] A. B. L. Tort, M. A. Kramer, C. Thorn, D. J. Gibson, Y. Kubota, A. M. Graybiel, and N. J. Kopell, "Dynamic cross-frequency couplings of local field potential oscillations in rat striatum and hippocampus during performance of a T-maze task," *Proceedings of the National Academy of Sciences*, vol. 105, no. 51, pp. 20 517–20 522, Dec. 2008.

[6] M. Kramer and U. Eden, "Assessment of cross-frequency coupling with confidence using generalized linear models," *Journal of Neuroscience Methods*, vol. 220, no. 1, pp. 64–74, Oct. 2013.

[7] S. M. Szczepanski, N. E. Crone, R. A. Kuperman, K. I. Auguste, J. Parvizi, and R. T. Knight, "Dynamic changes in phase-amplitude coupling facilitate spatial attention control in fronto-parietal cortex," *PLOS Biology*, vol. 12, no. 8, pp. 1–14, 08 2014.

[8] M. X. Cohen, C. E. Elger, and J. Fell, "Oscillatory Activity and Phase–Amplitude Coupling in the Human Medial Frontal Cortex during Decision Making," *Journal of Cognitive Neuroscience*, vol. 21, no. 2, pp. 390–402, 02 2008.

[9] T. O. Bergmann and J. Born, "Phase-Amplitude Coupling: A General Mechanism for Memory Processing and Synaptic Plasticity?" *Neuron*, vol. 97, no. 1, pp. 10–13, Jan. 2018.

[10] C. de Hemptinne, E. S. Ryapolova-Webb, E. L. Air, P. A. Garcia, K. J. Miller, J. G. Ojemann, J. L. Ostrem, N. B. Galifianakis, and P. A. Starr, "Exaggerated phase–amplitude coupling in the primary motor cortex in Parkinson disease," *Proceedings of the National Academy of Sciences*, vol. 110, no. 12, pp. 4780–4785, Mar. 2013.

[11] J. Wang, Y. Fang, X. Wang, H. Yang, X. Yu, and H. Wang, "Enhanced Gamma Activity and Cross-Frequency Interaction of Resting-State Electroencephalographic Oscillations in Patients with Alzheimer's Disease," *Frontiers in Aging Neuroscience*, vol. 9, p. 243, Jul. 2017.

[12] R. Zhang, Y. Ren, C. Liu, N. Xu, X. Li, F. Cong, T. Ristaniemi, and Y. Wang, "Temporal-spatial characteristics of phase-amplitude coupling in electrocorticogram for human temporal lobe epilepsy," *Clinical Neurophysiology*, vol. 128, no. 9, pp. 1707–1718, Sep. 2017.

[13] J. Aru, J. Aru, V. Priesemann, M. Wibral, L. Lana, G. Pipa, W. Singer, and R. Vicente, "Untangling cross-frequency coupling in neuroscience," *Current Opinion in Neurobiology*, vol. 31, pp. 51–61, Apr. 2015.

[14] M. A. Kramer, A. B. L. Tort, and N. J. Kopell, "Sharp edge artifacts and spurious coupling in EEG frequency comodulation measures," *Journal of Neuroscience Methods*, p. 6, 2008.

[15] J. I. Berman, J. McDaniel, S. Liu, L. Cornew, W. Gaetz, T. P. Roberts, and J. C. Edgar, "Variable Bandwidth Filtering for Improved Sensitivity of Cross-Frequency Coupling Metrics," *Brain Connectivity*, vol. 2, no. 3, pp. 155–163, Jun. 2012, publisher: Mary Ann Liebert, Inc., publishers.

[16] A. Hyafil, "Misidentifications of specific forms of cross-frequency coupling: three warnings," *Frontiers in Neuroscience*, vol. 9, 2015.

[17] T. Dupré la Tour, L. Tallot, L. Grabot, V. Doyère, V. Van Wassenhove, Y. Grenier, and A. Gramfort, *Non-linear Auto-Regressive Models for Cross-Frequency Coupling in Neural Time Series*, Nov. 2017.

[18] R. Martinez-Cancino, A. Delorme, K. Kreutz-Delgado, and S. Makeig, *Computing Phase Amplitude Coupling in EEGLAB: PACTools*, Oct. 2020, pages: 394.

[19] E. Combrisson, T. Nest, A. Brovelli, R. A. A. Ince, J. L. P. Soto, A. Guillot, and K. Jerbi, "Tensorpac: An open-source Python toolbox for tensor-based phase-amplitude coupling measurement in electrophysiological brain signals," *PLOS Computational Biology*, vol. 16, no. 10, p. e1008302, 2020.

[20] P. Welch, "The use of fast fourier transform for the estimation of power spectra: A method based on time averaging over short, modified periodograms," *IEEE Transactions on Audio and Electroacoustics*, vol. 15, no. 2, pp. 70–73, 1967.

[21] T. Donoghue, M. Haller, E. J. Peterson *et al.*, "Parameterizing neural power spectra into periodic and aperiodic components," *Nature Neuroscience*, vol. 23, pp. 1655–1665, 2020.

[22] M. Cohen, *Analyzing Neural Time Series Data: Theory and Practice*, 01 2014.

[23] A. Gramfort, M. Luessi, E. Larson, D. A. Engemann, D. Strohmeier, C. Brodbeck, R. Goj, M. Jas, T. Brooks, L. Parkkonen, and M. S. Hämäläinen, "MEG and EEG data analysis with MNE-Python," *Frontiers in Neuroscience*, vol. 7, no. 267, pp. 1–13, 2013.

[24] J. Timmer and M. Koenig, "On generating power law noise." *Astronomy and Astrophysics*, vol. 300, p. 707, 1995.

[25] S. Tsuchimoto, S. Shibusawa, N. Mizuguchi, K. Kato, H. Ebata, M. Liu, T. Hanakawa, and J. Ushiba, "Resting-state fluctuations of EEG sensorimotor rhythm reflect bold activities in the pericentral areas: A simultaneous EEG-fMRI study," *Frontiers in Human Neuroscience*, vol. 11, 2017.

[26] M. Chaumon, D. V. Bishop, and N. A. Busch, "A practical guide to the selection of independent components of the electroencephalogram for artifact correction," *Journal of Neuroscience Methods*, vol. 250, pp. 47–63, Jul. 2015.